Applied Water Science (2021) 11:93
https://doi.org/10.1007/s13201-021-01429-x

ORIGINAL ARTICLE

Hydrothermal fabrication and characterization of novel $CeO_2/PbWO_4$ nanocomposite for enhanced visible-light photocatalytic performance

S. Selvi[1] · Ranjith Rajendran[2] · N. Jayamani[1]

Received: 21 March 2021 / Accepted: 14 May 2021 / Published online: 22 May 2021

Abstract

In this revision, a series of novel visible-light-driven (VLD) $CeO_2/PbWO_4$ nanocomposites (NCs) were effectively fabricated by facile hydrothermal preparation way. The UV–Vis absorption spectra exposed that CeO_2 NPs prolonged the adsorption edge of the $CeO_2/PbWO_4$ composite to the extensive visible region, which allied to decreases of the bandgap. As-prepared $CeO_2/PbWO_4$ NCs revealed superior photocatalytic action under visible-light and could degrade the Methylene Blue (MB) dye solution in 140 min. The photodegradation efficacy of $CeO_2/PbWO_4$ NCs was improved catalytic activity, which is around 1.45 and 2.7 times that of CeO_2 and $PbWO_4$ nanoparticles (NPs) individually. Besides, the $CeO_2/PbWO_4$ catalysts display notable stability and reusability performance in four succeeding cycles. The development in the photocatalytic enactment of combined $CeO_2/PbWO_4$ nanocomposite could be recognized not only to the sturdy visible-light absorption responses and separating the photoexcited electron–hole pairs. Also, the plausibly systematic illumination of charge transference and exploitation of reactive species for superior photocatalytic action in visible-light have been discussed. It is projected that the $CeO_2/PbWO_4$ NCs could be used as effective photocatalysts for promising applications for environmental wastewater refinement.

Keywords $CeO_2/PbWO_4$ · Nanocomposites · Hydrothermal · Visible light · Photodegradation · Active species

Introduction

Over the former few years, water contaminants have industrial wastewater become the greatest challenging ecological concerns and thus aroused abundant courtesy in the progress of modern society (Gour and Jain 2019). Wastewater usually covers a huge amount of organic pollutants (such as reactive dyes, pesticides and antibiotics) which is adverse things on aquatic ecologies equilibrium and human healthiness. The textile, paper-making, cosmetics, food industries and dye houses have used countless organic dyes which are the prime causes for the contamination of environmental wastewater due to its toxicity and non-biodegradability is a vital environmental issue (Dhmees et al. 2019). Various traditional systems, such as electrochemical oxidation, membrane filtration, adsorption, chlorination, reverse osmosis, and photocatalysis, have been agreed to treat the harmful dyes covering wastewater. Amid these skills, semiconductors (SCs) based photocatalysis has drawn increasing interest because it offers a capable substitute strategy to eradicate the dye-containing wastewater since of its high efficacy, green reaction route and moderate reaction settings (Rohini et al. 2017) for solving the recent severe problems of environmental pollution and energy shortages. Unfortunately, the utmost of these physical, chemical and biological systems could custom to secondary impurities simply through degradation manners (Venkatasubramanian et al. 2008). The advanced oxidation practices (AOPs) of semiconductor photocatalysts (PCs) were broadly considered by deprivation of various noxious organic toxins in environment remediation and antimicrobial action (Girase et al. 2011; Depan and Misra 2014; Zhang et al. 2019b; Shanmugam et al. 2020). The photodegradation and mineralization of the dyes by nano-configuration semiconductor in visible-light treated progress has engrossed great concern in modern years. Various metal oxides (such as ZnO, TiO_2, Fe_2O_3, CeO_2, and WO_3) have been repeatedly employed as support in heterogeneous catalysis of organic pollutants degradation in the wastewater and antimicrobial activity (Rana et al. 2006; Rawat et al. 2007a;

✉ N. Jayamani
jayamaniphysics@gmail.com

[1] Department of Physics, Government Arts College (Autonomous), Salem, Tamilnadu 636001, India

[2] Department of Physics, Periyar University, Salem, Tamilnadu 636 011, India

Ke et al. 2008; Sunkara and Misra 2008; Xu and Wang 2012; Li et al. 2019).

As a significant rare earth metal oxide chains, cerium oxide (CeO_2), a wide bandgap SCs which fascinates light in the nearby UV and slightly visible region. Likewise, the CeO_2 has eco-friendly photocatalytic material, has encouraged abundant concern of the researchers owing to its favorable applications, for instance, plentiful oxygen sensors, luminescent things besides admirable chemical constancy, high catalytic action and cost-effective nature (Li et al. 2019; Qi et al. 2019). This material was also functional for solar water splitting (Ce^{4+}/Ce^{3+}) into hydrogen creation and concerned increasing attention used for deletion of organic pollutants from wastewater owed to its strong light captivation (Priyadharsan et al. 2017a). Though, the key weakness of CeO_2 is the absence of visible-light consumption since the large bandgap (2.92 eV) and weak separation efficacy of photoexcited carriers hinders have its widespread request in photocatalysis. Hence it is probable to outspread the visible-light captivation skill of CeO_2 either by doping of metals/nonmetals or fashioning a heterojunction between CeO_2 and another narrow bandgap SCs to create VLD PCs (Cano-Franco and Álvarez-Láinez 2019a). Unfortunately, the UV region signifies a little amount (3–5%) of photon flux whereas the visible region attains 45% of daylight. So that, it has required to progress the photocatalytic efficacy by doping or coupling the CeO_2 with narrow bandgap materials which could diminish the recombination of the photogenerated electron/hole pair rate and extend their lifetime important to the excellent light absorption from UV to the visible region for the elimination of organic pollutants (Ma et al. 2019). As a member of the tungstate family, lead tungstate ($PbWO_4$) is a scientific importance inorganic scintillating semiconductor, which has vast potential applications like humidity identical sensors, solid-state lasers ground, optical fibers, and catalysts (Pourmasoud et al. 2017; Rajendran et al. 2019). $PbWO_4$ is utmost smart for high-energy physics uses since of its great density (8.3 g/cm^3), short decay time (< 10 ns for a large part of light output), high-irradiation destruction resistance, exciting excitonic luminescence, thermo-luminescence, encouraged Raman scattering manners (Yue et al. 2016).

In this present effort, we report novel $CeO_2/PbWO_4$ heterojunction PCs that were effectively fabricated via a simplistic hydrothermal method. The as-obtained nanocomposites (NCs) were categorized by numerous analytical tools such as XRD, FTIR, HR-SEM, HRTEM, PL and UV-DRS spectroscopy were employed to study the crystalline formation, phase configuration, morphology, and optical possessions parallel with CeO_2 and $PbWO_4$ samples. The as-organized $CeO_2/PbWO_4$ NCs were used as a UV and/or visible-light focused photocatalyst towards the photodegradation of MB dye. Coupled with $PbWO_4$ on the superficial of CeO_2 NPs are projected to increase the surface area of composite providing further response sites owing to lower bandgap and so improve its photocatalytic action. Eventually, a reasonable mechanism and photostability of the catalyst are also anticipated in detail.

Experimental part

Materials

Lead nitrate hexahydrate ($Pb(NO_3)_3{\cdot}6H_2O$; 99%), Sodium tungstate dihydrate ($Na_2WO_4.2H_2O$, 99%), Ethylene glycol (99%) were procured from Himedia Ltd. Potassium chloride (Merck, 99%), Cerium nitrate, ($Ce(NO_3)_3{\cdot}6H_2O$; 98%) were obtained since SRL Chem. Limited. Sodium hydroxide (NaOH), isopropanol (IPA), Di-sodium Ethylene Diamine Tetra Acetic Acid (EDTA-2Na), benzoquinone (BQ), and absolute ethanol (CH_3CH_2OH) were acquired from SDFCL Chemical Reagent Co., Pvt. Ltd. Methylene blue (MB; $C_{16}H_{18}ClN_3S$) dye from SD Fine and was used as received. Deionized water (D.I) was used for the preparation of all solutions. All the chemicals were analytical reagent (A.R) grade also have auxiliary purified before use.

Preparation of $CeO_2/PbWO_4$ photocatalyst

In a typical synthesis, 0.03 mol of $Ce(NO_3)_3{\cdot}6H_2O$ was ultrasonically dissolved in 100 mL of D.I water, then 10 mL NH_4OH was gradually dropped directly into the above reaction mixture for pH extended at ~ 12 under constant stirring for 30 min. Lastly, the composed precipitants (Cui et al. 2019) were kept dry at 60 °C for 8 h and extra calcined at 400 °C for 1.5 h to attain CeO_2 NMs. In this research, the CeO_2 blended $PbWO_4$ NMs, via 0.03 mol of $Pb(NO_3)_3{\cdot}6H_2O$ and 0.03 mol of $Na_2WO_4.2H_2O$ solution was added by 50 ml of D.I water. And 1 mol (50 mL) of NH_4OH solution was additional in the pioneer solution, although the pH value was touched at ~ 11–12. Afterwards, being stirred for 3 h, the 0.1 g of as-obtained CeO_2 NMs was auxiliary added in the upstairs produces and formerly stirred for 2 h. Then, the reaction mixer was relocated to heat-treat by 160 °C aimed at 24 h in a 250 mL Teflon-lined stainless steel autoclave. Lastly, the autoclave was then cooled to room temperature, hence the as-attained $CeO_2/PbWO_4$ precipitate was centrifugated and rinsed carefully with ethanol/D.I. water further dry at 70 °C for 8 h. Besides, the $CeO_2/PbWO_4$ NCs was attained (Jeyakanthan et al. 2018). Advising to this outline, the pristine $PbWO_4$ NPs was also attained via without accumulation of CeO_2 NMs.

Characterization of the obtained samples

The crystal organization and phase of as-obtained nanocomposite was estimated by X-ray diffraction (Rigaku Miniflex-II; X-ray diffractometer) over CuKα radiation in the 2θ range from 10 to 80°. FTIR revisions were done by Perkin Elmer RX-1 FTIR spectrophotometer. Surface morphologies and microstructure of as given NMs were scrutinized via high-resolution (HR-SEM; HITACHI S-3000 H) scanning electron microscope and high-resolution transmission electron microscopy (HR-TEM; JEM-2011; JEOL-Japan) instruments. Energy-Dispersive X-ray spectroscopy (EDX-attached with HRSEM) was used to evaluate the elemental compositions of the NCs. To measure the optical assets of the attained samples were considered by a UV–Vis DRS spectrophotometer (UV2550 model, Shimadzu—Japan). Photoluminescence (PL) spectrophotometry was performed with a (Perkin-Elmer-LS 100) to determine the electron–hole recombination rate at an excitation series of ~ 342 nm. The optical absorption of dye degradation samples was performed via a UV–Vis spectrophotometer (UV; Perkin-Elmer Lambda-19). The absorption spectra in the photodegradation rate process of MB dye solutions also measured with a UV–Vis (Perkin Elmer-Lambda 35) spectrometer.

Description of the photocatalytic activity of MB dye

The photodegradation performing of as-attained samples (50 mg) was measured via deprivation of MB dye (20 ppm; 100 mL solution; 10 mg/L) under visible-light exposure (300 W Xe lamp by $\lambda > 420$ nm cutoff filter in a Pyrex photocatalytic vessel). Preceding to exposure, the suspensions stayed constant magnetically stirred for around 30 min in the dark to certify that the dyes might extend the absorption–desorption balance on the photocatalyst superficial and dyes (Ali Baig et al. 2020). At certain time pauses of 20 min irradiation, 2.5 mL of aliquots were collected. The degraded resolutions were explored by UV–Vis absorption peaks of corresponding MB dye (wavelength at ~ 663.5 nm) (Zeleke and Kuo 2019). The photodegradation efficacy was extent as resulting formula, Efficiency (%) = $(C_0\text{-}C_t)/C_0$*100, wherever C_0 and C_t exist the absorbance rate of dyes solution earlier and afterwards destruction. Finally, through the degradation manner, photocatalyst was separated from the reaction blend and dried to succeed in the reusability trials (Zhang et al. 2017).

Active species trapping experiments

To detect that the reactive species, certain caused/trapping mechanism during the photocatalytic manner, 1 mM of EDTA-2Na IPA and BQ and were added as scavengers of holes (h^+) hydroxyl radicals (% $\bullet OH^-$) and superoxide radical (% $O_2\bullet^-$) exclusively surveyed by the photocatalytic valuations, hence to catch the detection of dynamic reactive species (Cardillo et al. 2016).

Results and discussion

Crystal structure investigation

To explore the crystal constructions and phase composition of the as-obtained samples, XRD evaluations were carried out. As exposed in Fig. 1a, the key diffraction peaks are indexed to the (111), (200), (220), (311), (222), (400) and (311) crystal planes, which was in moral contract with the typical cubic crystalline phase structure pattern of CeO_2 (JCPDS card No: 89-8436) (Syed Khadar et al. 2019). For $PbWO_4$, the diffraction peaks (Fig. 1b) and consistent planes of (112), (004), (200), (204), (220), (116) and (312), respectively, could be well-indexed to the pure tetragonal stolzite phase (JCPDS card No. 19-0708) (Xiong et al. 2015). In Fig. 1c, designating a good crystallinity of CeO_2/$PbWO_4$ NCs revealed the association with both the distinctive diffraction peaks of CeO_2 and $PbWO_4$ crystalline phases. The solid and sharp diffraction peaks proposed that the CeO_2/$PbWO_4$ nanocomposite was fine crystalline in nature. No characteristic impurity peaks from other crystalline forms were detected which proves that the CeO_2/$PbWO_4$ NCs has high purity. The average crystallite size (D) of as-prepared NCs was intended by the full width half maximum (FWHM) using Scherer's equation (Ramos-Corella et al. 2019), The average crystalline sizes for the pristine CeO_2, $PbWO_4$ and CeO_2/$PbWO_4$ nanocomposite was found to be 24, 28 and 21.5 nm, individually. The intensity variance and peak extending of the CeO_2/$PbWO_4$ NCs are ascribed to a substantial reduction of crystallite sizes (Table 1).

FT-IR analysis

To decide the proper functional groups in final catalysts samples, FT-IR spectra of as-obtained CeO_2, $PbWO_4$ and CeO_2/$PbWO_4$ NCs were perceived in the series of 400–4000 cm^{-1} and shown in Fig. 2. An exact extensive band of 3100–3650 cm^{-1} is recognized to the typical surface hydroxyl (O–H) stretching mode (Saravanakumar et al. 2019). The bending vibration group of actually adsorbed water (H_2O) molecules are besides observed at 1635–1670 cm^{-1} band. An increase in the number of surfaces -OH groups could expand the photocatalytic action. The existence of sharp dominated absorption peaks on 570–730 cm^{-1} which is linked to the metal-O (Ce–O, W–O, Pb–O) bonds/stretching vibration are confirmed that the prepared NCs (Syed Khadar et al. 2019). Usually, spinel oxide and metal–oxygen broadening frequencies are perceived in

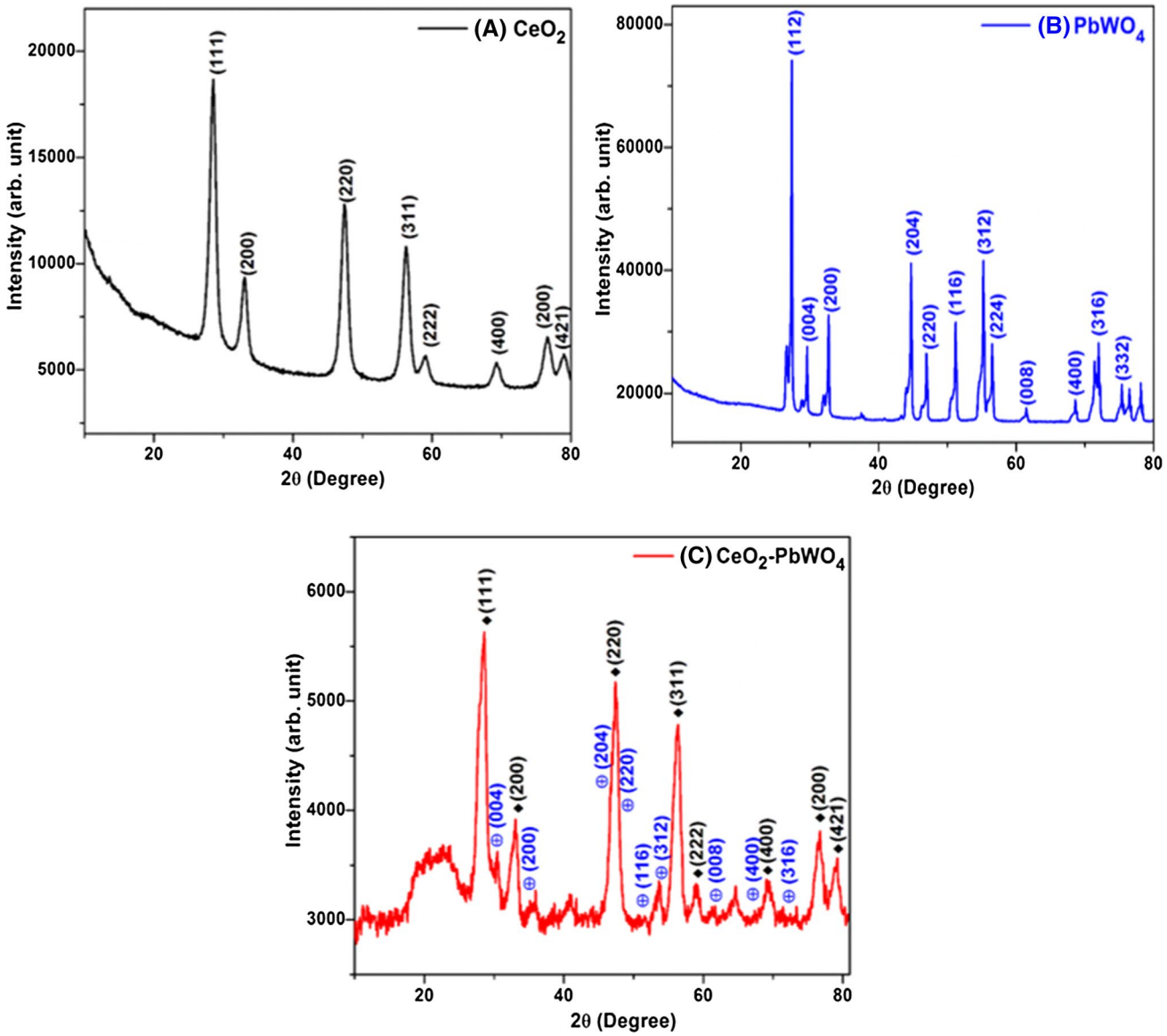

Fig. 1 XRD pattern of as obtained nanomaterials

Table 1 Comparison of visible-light assisted MB dye photodegradation rate (%) over earlier reported nanocomposite materials

S. No	Nanomaterials	Irradiation time (mins.)	Degradation efficiency (%)	References
1	CeO_2	180	86	(Reddy Yadav et al. 2017)
2	$NiWO_4$	330	60	(AlShehri et al. 2017)
3	g-C_3N_4/$BaTiO_3$	360	76	(Xian et al. 2015)
4	g-C_3N_4/CeO_2	120	74	(Kumar et al. 2013)
5	CdS/TiO_2	310	62	(Wei et al. 2014)
6	α-Fe_2O_3/TiO_2	160	80	(Li et al. 2016)
7	CeO_2/$PbWO_4$	140	94	This work

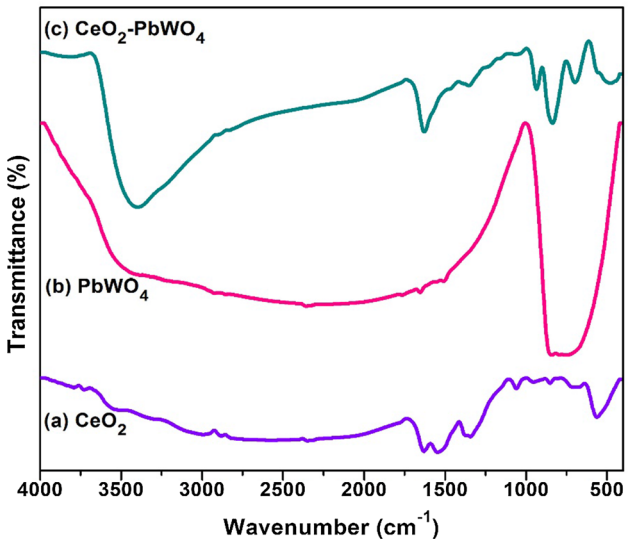

Fig. 2 FT-IR spectra of as-prepared samples

the peak range of 650–850 cm^{-1}. No auxiliary absorption group was sensed in the experimental FTIR spectrum (Rana et al. 2005b).

Morphology and microstructure analysis

To acquire detailed evidence about exterior morphology and microstructure of the CeO_2, $PbWO_4$ and $CeO_2/PbWO_4$ NCs were inspected by HRSEM and HRTEM. Figure 3a the HRSEM images of pristine CeO_2 demonstrates spherical shaped aggregates morphology. Figure 3b for $PbWO_4$ shows a uniform ball-shaped structure was obtained. Also the Fig. 3c the $CeO_2/PbWO_4$ NCs displays the high agglomeration of CeO_2 NPs rendered with non-uniform spherical fashioned aggregates (Ramasamy Raja et al. 2019). The elemental composition and purity analysis of $CeO_2/PbWO_4$ NCs have been determined from EDX extents. The EDX inquiry authorizes the existence of all essential elements

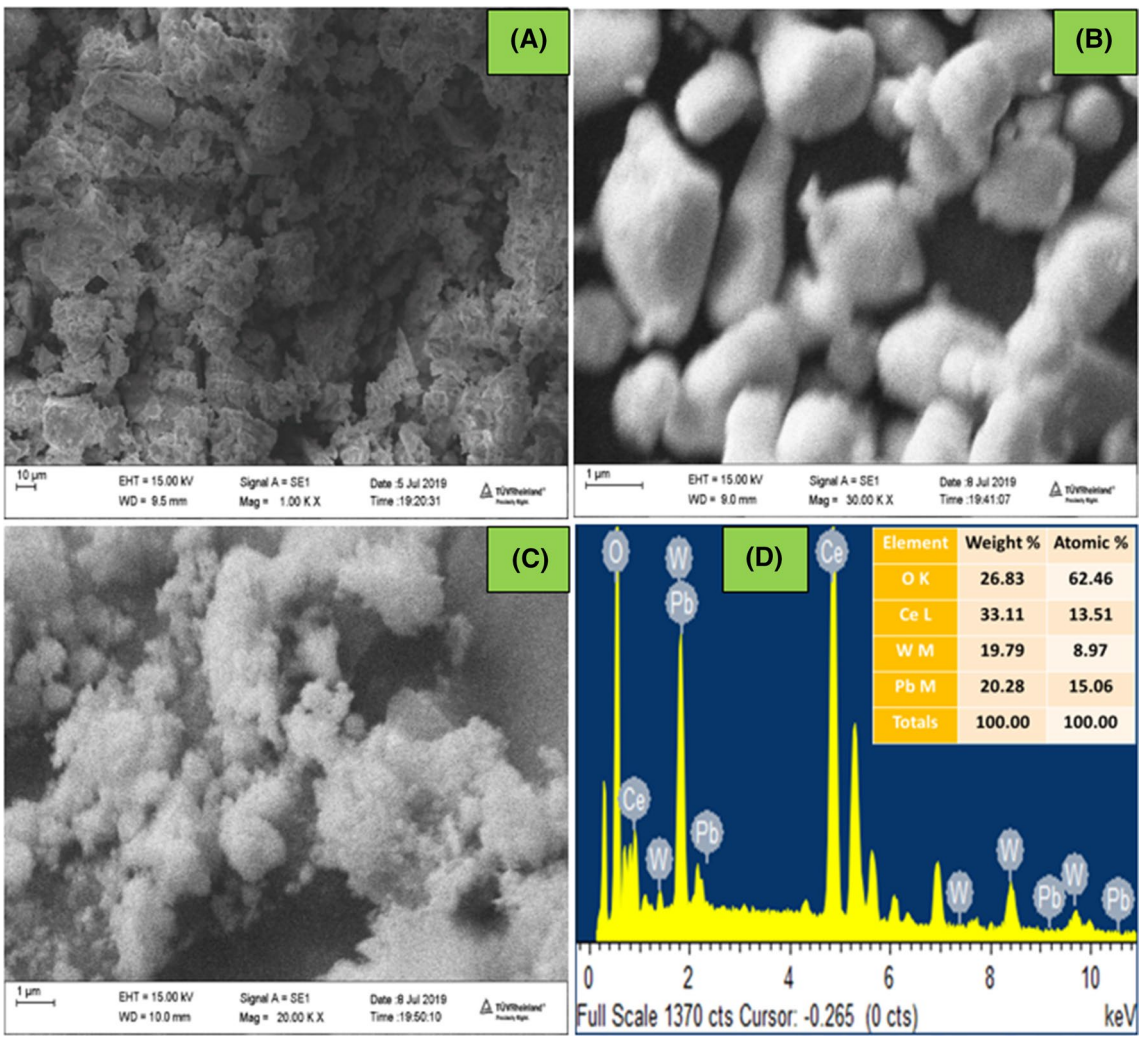

Fig. 3 HRSEM micrographs of as-synthesized **a** CeO_2 **b** $PbWO_4$ **c** $CeO_2/PbWO_4$ NCs and **d** EDX spectrum of the $CeO_2/PbWO_4$ NCs

such as Ce, W, Pb, and O individually from $CeO_2/PbWO_4$ NCs as described in Fig. 3d, also the weight % are detected and inserted in Fig. 3d (Lan et al. 2018). Moreover, the EDX elemental mapping analysis characterizes that the distribution of W, Ce, O and Pb elements separately and as illustrated in Fig. 4. It is well evident that $PbWO_4$ and CeO_2 are evenly circulated in the $CeO_2/PbWO_4$ NCs. Furthermore, the EDX spectra and corresponding elemental mapping outcomes of as-obtained $CeO_2/PbWO_4$ NCs which are very pure and no other impurities are found. The HRTEM analysis of $CeO_2/PbWO_4$ NCs is publicized in Fig. 5a–b. The HRTEM micrograph indicates that the number of CeO_2 fine NPs has indeed deposited compactly on the $PbWO_4$ surface structure and also homogeneous dispersion nature were forming the nano-sized composite (Aboutaleb and El-Salamony 2019). Moreover, the surface has several irregular small granules with additional agglomeration and the shape is more or less spherical. The intimate contact amid $PbWO_4$ and CeO_2 facilitates the separation of the photoexcited carriers, which favours the enhancement of photocatalytic concert (Hezam et al. 2017).

Optical properties

The optical properties and energy bandgap of the as-obtained samples have very important to determine the

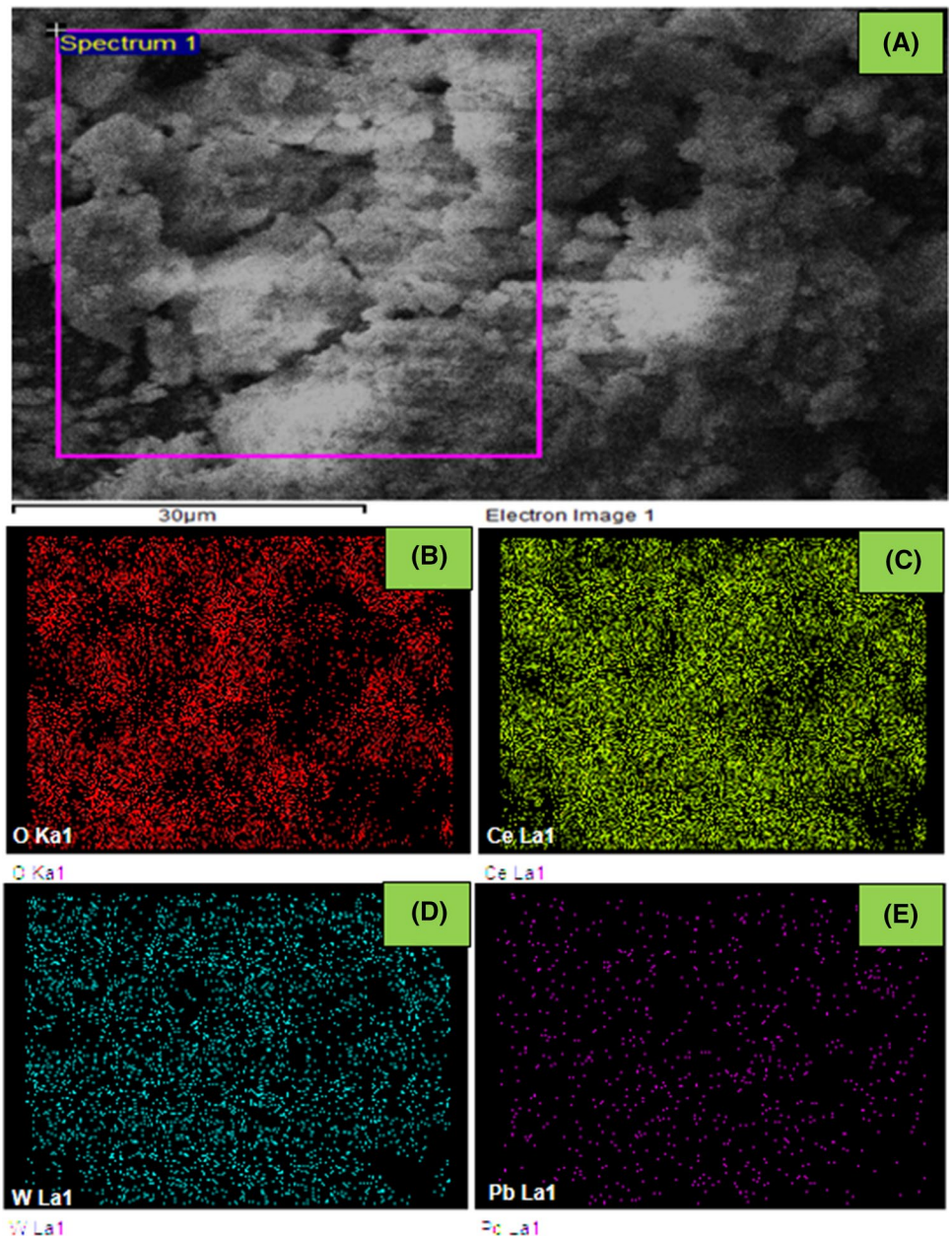

Fig. 4 EDX elemental mapping analysis of $CeO_2/PbWO_4$ nanocomposite

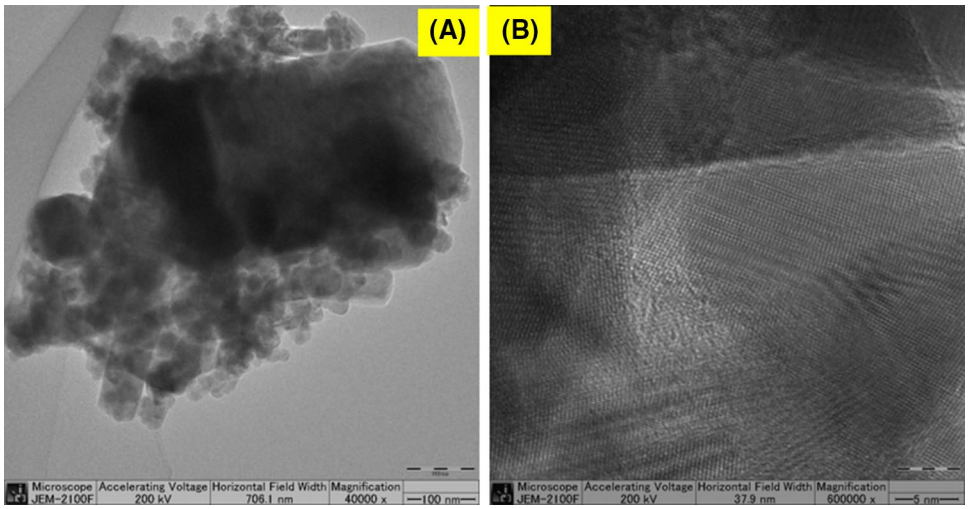

Fig. 5 HRTEM images of as-obtained $CeO_2/PbWO_4$ NCs

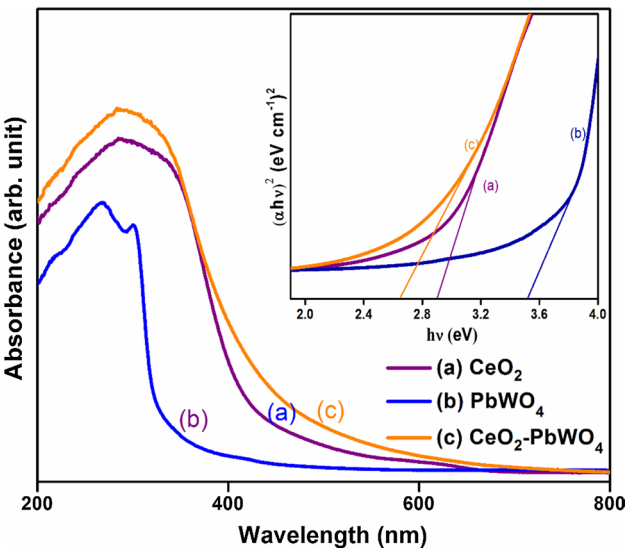

Fig. 6 **a** UV–Vis DRS absorption spectra **b** Tauc's plots of the CeO_2, $PbWO_4$ and $CeO_2/PbWO_4$ NCs

photocatalytic behaviors (Liang et al. 2017) were studied by UV–Vis DRS as exhibited in Fig. 6. The CeO_2, $PbWO_4$ and $CeO_2/PbWO_4$ nanomaterials (NMs) were shown in strong absorption ability in the wavelength range of 200–800 nm. Related with pristine CeO_2 and $PbWO_4$, the $CeO_2/PbWO_4$ NCs consume broader absorption competence (Rana et al. 2005a; Cano-Franco and Álvarez-Láinez 2019b), which is superior visible-light harvesting capacity and redshift (~ 290–418) of absorption edge implying that the $CeO_2/PbWO_4$ NCs owns admirable visible-light dynamic photocatalytic action (David et al. 2018; Wang et al. 2019). The bandgap energy was determined by fitting the absorption facts since the direct transition equation, $(\alpha h\nu) = A(h\nu\text{-}Eg)^n$, where h refers the Planck's constant, α stands for absorption coefficient, E_g stands for bandgap (eV), ν has shorted in the frequency of vibration, A is the relatively constant. Also, n refers could have values ½ and 2 contingent on the kind of inter-band conversion, i.e., direct and indirect allowed transition, individually. The bandgap energy (E_g) values are optically deduced from the Tauc plots and the graph plotted by $(\alpha h\nu)^2$ versus the photon energy (hν). The E_g values of CeO_2, $PbWO_4$ and $CeO_2/PbWO_4$ heterojunction NCs are nearly 2.92, 3.52 and 2.68 eV, separately were exposed in insert of Fig. 6. However, the CeO_2 combined $PbWO_4$ NCs could reduce the bandgap energy of $CeO_2/PbWO_4$ NCs which is owed to an energy transition since the visible region triggered by an active band of $PbWO_4$ effectively deposited on the CeO_2 surface (Liu et al. 2019). In the combined effect of light, absorption would have an obvious effect while catalytic action towards the degradation of dyes qualified to absorption of quite visible-light to probably make more charge carriers (Velusamy and Lakshmi 2017).

Photoluminescence analysis

The photoluminescence (PL) system is also an effective approach to assess the separation ability of photoexcited electron–hole (e^--h^+) pairs since it directly related to photocatalytic efficacy. The PL spectrum of the as-synthesized pristine CeO_2, $PbWO_4$ and $CeO_2/PbWO_4$ heterojunction NCs were investigated as shown in Fig. 7. The PL emission intensity of $CeO_2/PbWO_4$ nanocomposite was lesser than that of pristine CeO_2 and $PbWO_4$, signifying that the coupling of $PbWO_4$ NPs might reduce the fluorescence from the CeO_2 NPs while the recombination rate of (e^--h^+) pairs is seriously reserved and extend the lifetime of charge carriers (Jeyakanthan et al. 2018). It is well established that coupling of $PbWO_4$ NPs onto the superficial of CeO_2 donated for reduced recombination rate of photoexcited charges related to CeO_2. This reduction might be accredited to (i) a greater amount of nominal defects and (ii) effectual charge

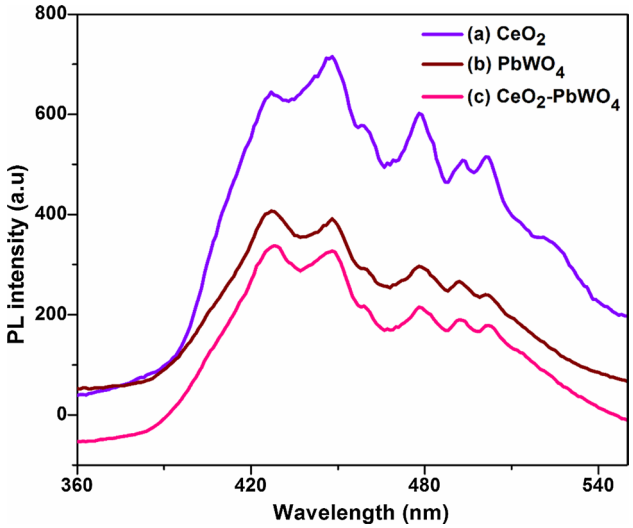

Fig. 7 Photoluminescence emission spectra of as-prepared samples

separation of CeO_2/$PbWO_4$ NCs (Koli and Kim 2019). The detected stronger characteristic PL near-band-edge emissions ranges of ~ 440–510 nm (448, 487 and 503 nm) for the visible region (apparently excitation peak at ~ 342 nm). Normally, the effective charge separation and inhibited (e^--h^+) recombination rate by coupling of CeO_2/$PbWO_4$ NCs was auspicious for enhancing the photocatalytic efficacy of CeO_2 NPs (Lu et al. 2020).

Photocatalytic activity

The photocatalytic performance was verified against the deprivation of MB aqueous dye in the existence of as-synthesized CeO_2, $PbWO_4$ and CeO_2/$PbWO_4$ PCs under visible-light exposure. It is seen from Fig. 8a, the characteristic UV–Vis absorption peak of MB dye solution at ~ 663.5 nm has constantly reduced by CeO_2/$PbWO_4$ photocatalyst and hence the supreme degradation efficacy almost 94% was degraded within 140 min. The photocatalytic proficiency of pristine CeO_2 and $PbWO_4$ for MB dye degradation was 42% and 58% in identical exposure time separately. The C/C_0 (where C_0 = absorption intensity of the initial dye solution and C = main absorption peak intensity of dye) has schemed vs. the wavelength as exposed in Fig. 8b. Related to the blank photodegradation testing of MB dye showed almost no obvious degradation in presence of a catalyst under the dark condition, along with an absence of catalyst and without catalyst in the light source, hence the curves could be neglected (Wen et al. 2018). Mostly, the MB organic dyes could be photodegraded by three conceivable reactions containing photolysis, photosensitization, and photocatalysis also. Largely, degradation efficacy was improved via accumulation of CeO_2/$PbWO_4$ photocatalyst effort might be the outcomes from (i) synergetic influence of the two metal oxides, (ii) leads to the decreases of bandgap energy, (iii) hindrance of the recombination rate of photoexcited (e^--h^+) pairs separation amid CeO_2 and $PbWO_4$ heterojunction, (iv) accessibility of surface reactive sites, (v) development of light absorption ability of photoexcited charges generated in the visible-light (Rawat et al. 2007b). The primary absorbance of the peak disappeared entirely after 140 min of visible-light exposure in the CeO_2/$PbWO_4$ photocatalyst which specifies the cleavage of conjugated chromosphere structure of MB dye and exchange into small aromatic intermediary (Rožić et al. 2019).

Kinetics of MB dye photodegradation

The photocatalytic reaction kinetics of MB dye in visible-light, overall the photocatalysts, was considered by a

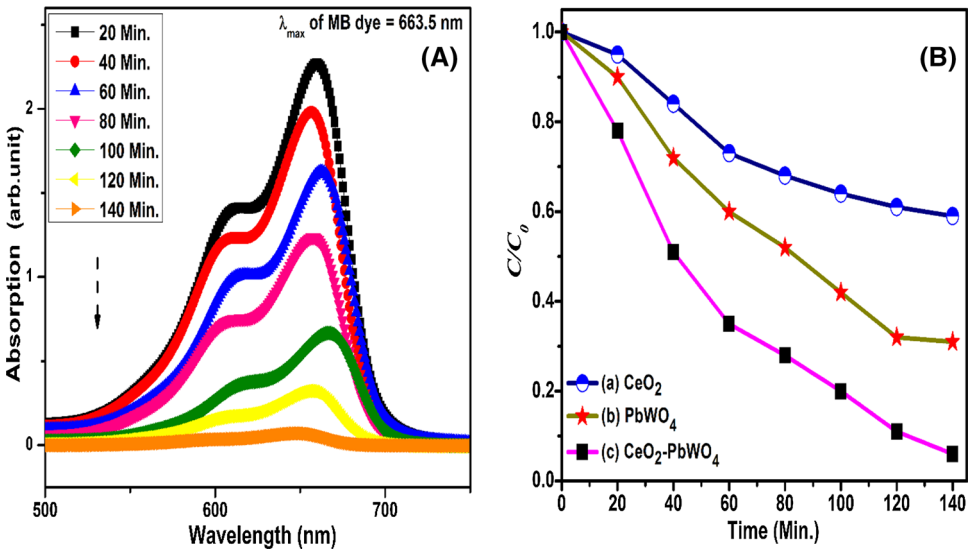

Fig. 8 **a** UV–Vis absorption spectra of MB dye solution using CeO_2/$PbWO_4$ NCs under visible-light exposure **b** Photodegradation rate of prepared photocatalysts

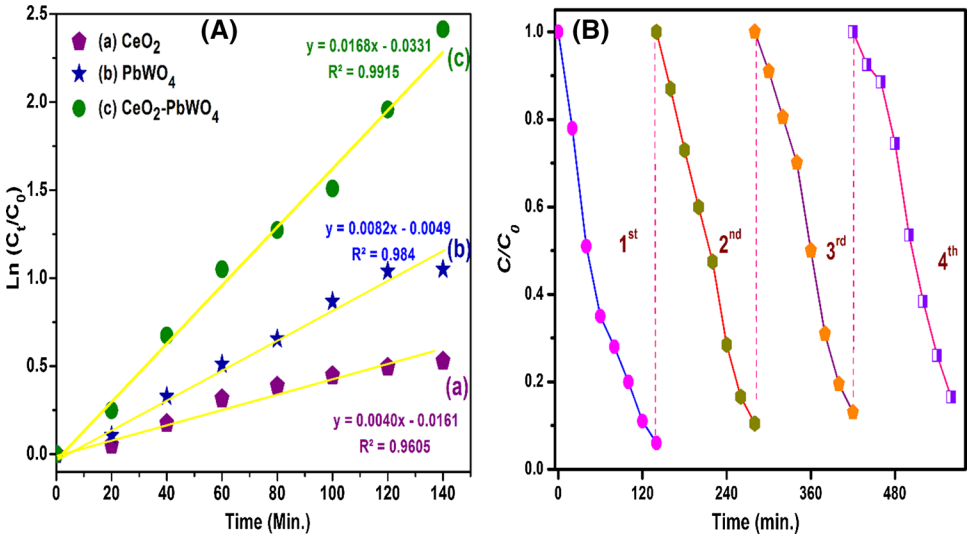

Fig. 9 **a** Photodegradation linear plot ln (C_0/C_t) versus time of as-prepared photocatalytic samples **b** Reusability performance of $CeO_2/PbWO_4$ photocatalyst

consistent pseudo-first-order kinetic equation of $\ln C_0/C_t = kt$ using CeO_2, $PbWO_4$ and $CeO_2/PbWO_4$ PCs as shown in Fig. 9a. Here, k refers to a reaction rate constant, C_0 and C_t are the initial and residual concentrations of MB aqueous dye solution at the agreeing time, and t (min) was initiate to be linear regression (Yu et al. 2013; Xu et al. 2020). The obvious rate constants for CeO_2, $PbWO_4$ and $CeO_2/PbWO_4$ PCs were calculated as 0.0004, 0.0082, and 0.0164 min^{-1}. The k value has increased in the order of $CeO_2 < PbWO_4 < CeO_2/PbWO_4$. It has decided that $CeO_2/PbWO_4$ PCs has a greater rate constant and it has 4.2 and 2.1 fold enrichment linked to that of pristine CeO_2 and $PbWO_4$ PCs, separately. Also, the $CeO_2/PbWO_4$ NCs owns expressively high photocatalytic dye degradation effectiveness as compared with related metal oxides and reported in other nanocomposites (Kumar et al. 2013; Wei et al. 2014; Xian et al. 2015; Li et al. 2016; AlShehri et al. 2017; Reddy Yadav et al. 2017).

Reusability of the photocatalyst

To further explore the stability and reusability were of great consequence factor for its practical application, and the Fig. 9(b) has exhibits the recycling investigates of chief $CeO_2/PbWO_4$ PCs was repeatedly used (Shanmugam et al. 2019). For both cycles, the $CeO_2/PbWO_4$ PCs were recycled via centrifuging, washing and drying for the next cycling runs. For the $CeO_2/PbWO_4$ PCs, the MB dye photodegradation still existing good stability with only about 5% decreases from the initial activity (94%) during the 4th recycle. The activity loss has which largely might be owed to the photo-corrosion of the catalyst by light in $CeO_2/PbWO_4$ photocatalyst (Yu et al. 2015). As well, the XRD and FTIR analysis of $CeO_2/PbWO_4$ PCs were surveyed further to prove the stability of before and after the photocatalytic replies were carried out. As shown in Fig. 10a, b the XRD and FTIR

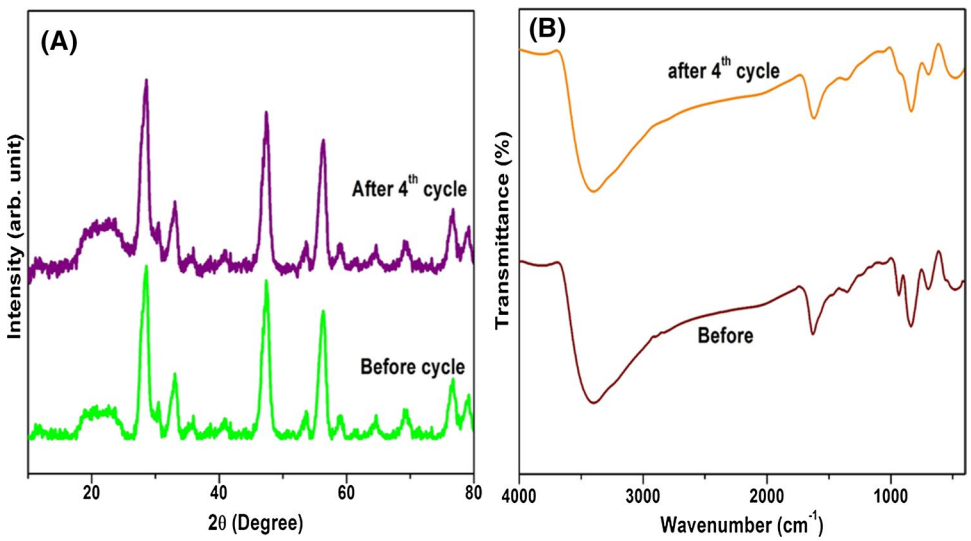

Fig. 10 **a** XRD pattern **b** FTIR spectra of before and after catalytic reacted photocatalyst

outcomes might designate that no notable changes are witnessed after 4th recycles, representing the structural stability of the $CeO_2/PbWO_4$ PCs has measured (Saravanakumar et al. 2016). These consequences propose that the $CeO_2/PbWO_4$ PCs used as effective superior photo-stability, and suitable recyclable PCs might also be reused constantly for wastewater treatment under visible-light contact (Vignesh et al. 2019).

Reactive species study

As well known, to validate the radicals of nanocomposites in the photodegradation progression, the trapping tests of reactive species are executed by utilizing light drive. Photo-excited (e^--h^+) pairs thereby form numerous reactive species for instance (% $O_2\bullet^-$) and hydroxyl radical (% $\bullet OH^-$), hence these reactive species could source in the decomposition of the organic toxins (Negi et al. 2019). Figure 11 as could be seen that photodegradation rate of as-obtained PCs has faintly reductions resultant from the adding of EDTA-2Na, hence validating that h^+ are not a major reactive species in this concerned systems. Likewise, the degradation rate is slightly declined when the addition of IPA, hence the % $\bullet OH^-$ is minor/deliberate part of the allied photocatalytic system. This is because the (VB) valence band potential of CeO_2 and $PbWO_4$ NPs have conjugated into the % $OH/\bullet OH^-$ also being % $\bullet OH^-$ cannot be fashioned. Though, the addition of BQ initiated significantly suppress the photocatalytic movement from 91 to 26% as presented in the tentative results. Based on the trapping investigation effects, it's resolved that % $O_2\bullet^-$ radicals are the dominant reactive species ($O_2 + e^- = \%\ O_2\bullet^-$) accountable for the decomposition of $CeO_2/PbWO_4$ photocatalytic scheme (Ravishankar et al. 2015).

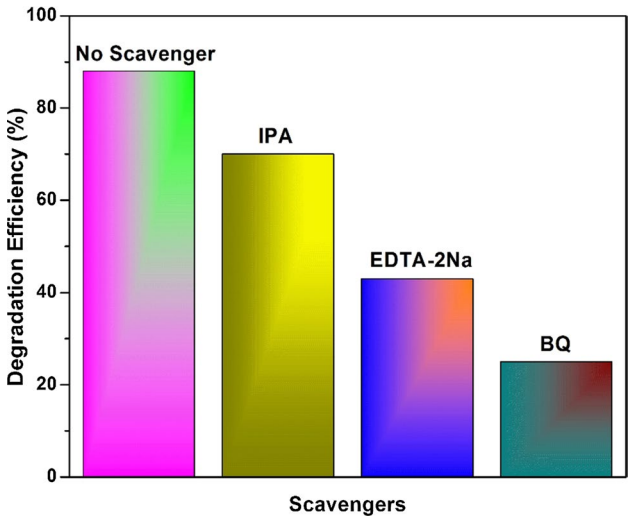

Fig. 11 Effect of scavengers on the MB dye photodegradation process

Possible photocatalytic mechanism

To obtain better consideration on the $CeO_2/PbWO_4$ PCs heterojunction, their valence band (VB) and conduction band (CB) edge potentials were intended via Mulliken electronegativity theory from the Eqs. (1) and (2)

$$E_{VB} = \mathrm{X} - E_e + 0.5E_g \quad (1)$$

$$E_{\mathrm{CB}} = E_{\mathrm{VB}} - E_g \quad (2)$$

wherever χ states the absolute electronegativity of certain semiconductors (χ is 5.56, 6.15 eV for CeO_2 and $PbWO_4$, singly). And the E_{VB}, E_{CB}, E_g and E_e are VB potential, CB potential, estimated optical bandgap of CeO_2 and $PbWO_4$, and energy of free electrons vs. hydrogen scale (4.5 eV), separately (Channei et al. 2019). Agreeing to the beyond equations, the E_{VB} and E_{CB} band edge potential values were assessed to be + 2.52 and − 0.11 eV for CeO_2 and as − 0.40 and + 3.41 eV for $PbWO_4$, separately. From the above-mentioned results, the probable photocatalytic mechanism (Fig. 12) comprises by visible-light which leads to the conception of a photoexcited electron (e^-) flowing towards CB of CeO_2 and thereby the VB of $PbWO_4$ acts as a drop for the hole (h^+) (Tomova et al. 2015). Thus, the e^- and h^+ could be proficiently divided; the e^--h^+ pairs are essentially gathered in the CB of CeO_2 and the VB of $PbWO_4$, individually. It is important to note that Ce element has two valence state (Ce^{4+} and Ce^{3+}), and Ce^{4+}/Ce^{3+} combine owns with multiple roles in endorsing the separation of photoexcited e^--h^+ pairs of $CeO_2/PbWO_4$ PCs, by which the photocatalytic performance is enriched (Misra et al. 2012; Priyadharsan et al. 2017b; Wang and Tian 2020). Essentially, Ce^{3+} could effortlessly trap the $O_2\bullet^-$ making chemical adsorption of oxygen on the exterior of CeO_2 centered on the $Ce^{3+} + O_2 = Ce^{4+}$—% $O_2\bullet^-$, which stimulates photocatalytic oxidation response. Instead of Ce^{3+}, which comprises oxygen defects could also absorb visible-light to harvest the photoexcited electron (e^-) (Ali Baig et al. 2021). All these gathered electrons (e^-) and Ce^{3+} own a strong reduction capacity was augmented easily and speedily decrease the absorbed O_2 on CeO_2 to cause active superoxide (% $O_2\bullet^-$) radicals (Cano-Franco and Álvarez-Láinez 2019). This is because the VB band edge potential of CeO_2 (+ 2.52 eV vs. NHE) develops more positive than $PbWO_4$ (-0.11 eV vs. NHE), which is beneficial for MB dye deprivation (Fukumura et al. 2017). While electron in the CB supports an O_2 molecule to form an $O_2\bullet^-$ radicals and formerly $O_2\bullet^-$ will respond with surface water molecules (H_2O) to yield the $\bullet OH^-$ radical. Lastly, the reactive radicals respond with MB dye molecules decayed to the intermediates or degradation yields over the highly oxidizing species ($O_2\bullet^-$, $\bullet OH^-$ etc.). The appropriate photocatalytic reaction progression (Reddy

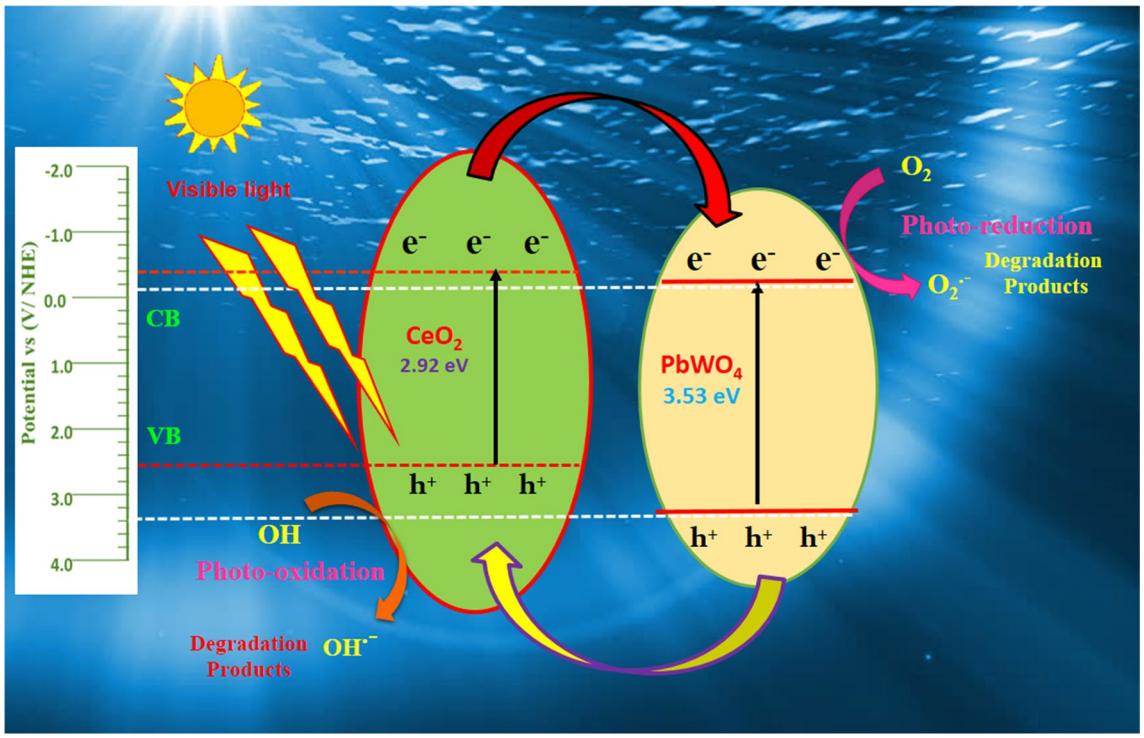

Fig. 12 Possible mechanism for the photoexcited electron–hole separation of the degradation of MB dye by $CeO_2/PbWO_4$ photocatalytic interface under visible-light

Yadav et al. 2016; Zhang et al. 2019a) could be also agreed upon by the succeeding Eqs. (3–7)

$$CeO_2/PbWO_4 + \text{Dye} + \text{Light} \rightarrow CeO_2/PbWO_4 + \text{Dye} + \left(e^-(\text{CB}) + h^+(\text{VB})\right) \quad (3)$$

$$\text{Dye} + e^-(\text{CB}) \rightarrow \text{Reduction Products} \quad (4)$$

$$\text{Dye} + h^+(\text{VB}) \rightarrow \text{Oxidative Products} \quad (5)$$

$$\text{Dye} + \text{OH} \rightarrow \text{OH}^{\cdot -} + \text{DegradationProducts} \quad (6)$$

$$\text{Dye} + O_2 \rightarrow O_2^{\cdot -} + \text{Degradation Products} \quad (7)$$

Conclusions

To sum up, $CeO_2/PbWO_4$ heterojunction photocatalyst was effectively formed via a facile and effectual hydrothermal scheme. The $CeO_2/PbWO_4$ nanocomposite was characterized by a range of techniques to study its phase purity, surface morphology, chemical composition and optical belongings were examined and debated in detail. In specific, $CeO_2/PbWO_4$ photocatalyst displayed the utmost photodegradation efficacy for 94% of MB aqueous dye within 140 min in visible-light treatment which is greater than other as-obtained samples. The degradation rate constant was closely 4.2 and 2.1 fold greater than those of pristine CeO_2 and $PbWO_4$ PCs singly. Also, •OH radicals were enabled in the key reactive species in the photodegradation route and the plausible degradation pathways have also been projected. Moreover, the optimized $CeO_2/PbWO_4$ photocatalyst presented an outstanding photocatalytic steadiness also reusability upto four consecutive cycles. The developed photocatalytic activities were recognized to the pairing of CeO_2 and $PbWO_4$ NPs were initiated by superior charge separation/transfer, reduced bandgap, and strong visible-light absorption proficiency thus suppressing the recombination of photoexcited charges. This study promotes the novel $CeO_2/PbWO_4$ NCs with outstanding visible-light photocatalytic action

and admirable stability was estimated to inspire potential environmental applications in may near future.

Funding The author(s) received no specific funding for this work.

Declarations

Conflict of interest The authors have declared no conflict of interest.

References

Aboutaleb WA, El-Salamony RA (2019) Effect of Fe2O3-CeO2 nanocomposite synthesis method on the Congo red dye photodegradation under visible light irradiation. Mater Chem Phys 236:121724. https://doi.org/10.1016/j.matchemphys.2019.121724

Ali Baig AB, Rathinam V, Palaninathan J (2020) Photodegradation activity of yttrium-doped SnO2 nanoparticles against methylene blue dye and antibacterial effects. Appl Water Sci 10:76. https://doi.org/10.1007/s13201-020-1143-1

Ali Baig AB, Rathinam V, Palaninathan J (2021) Facile synthesis of Ce-doped SnO2 nanoparticles with enhanced performance for photocatalytic degradation of organic dye. J Iran Chem Soc 18:13–27. https://doi.org/10.1007/s13738-020-02000-2

AlShehri SM, Ahmed J, Alzahrani AM, Ahamad T (2017) Synthesis, characterization, and enhanced photocatalytic properties of NiWO 4 nanobricks. New J Chem 41:8178–8186. https://doi.org/10.1039/C7NJ02085F

Cano-Franco JC, Álvarez-Láinez M (2019) Effect of CeO2 content in morphology and optoelectronic properties of TiO2-CeO2 nanoparticles in visible light organic degradation. Mater Sci Semicond Process 90:190–197. https://doi.org/10.1016/j.mssp.2018.10.017

Cardillo D, Weiss M, Tehei M et al (2016) Multifunctional Fe 2 O 3 /CeO 2 nanocomposites for free radical scavenging ultraviolet protection. RSC Adv 6:65397–65402. https://doi.org/10.1039/C6RA10951A

Channei D, Chansaenpak K, Jannoey P, Phanichphant S (2019) The staggered heterojunction of CeO2/CdS nanocomposite for enhanced photocatalytic activity. Solid State Sci 96:105951. https://doi.org/10.1016/j.solidstatesciences.2019.105951

Cui Z, Zhou H, Wang G et al (2019) Enhancement of the visible-light photocatalytic activity of CeO 2 by chemisorbed oxygen in the selective oxidation of benzyl alcohol. New J Chem 43:7355–7362. https://doi.org/10.1039/C9NJ01098J

David TM, Wilson P, Mahesh R et al (2018) Photocatalytic water splitting of TiO2nanotubes powders prepared via rapid breakdown anodization sensitized with Pt, Pd and Ni nanoparticles. Mater Technol 33:288–300. https://doi.org/10.1080/10667857.2018.1433349

Depan D, Misra RDK (2014) On the determining role of network structure titania in silicone against bacterial colonization: mechanism and disruption of biofilm. Mater Sci Eng C 34:221–228. https://doi.org/10.1016/j.msec.2013.09.025

Dhmees AS, Rashad AM, Eliwa AA, Zawrah MF (2019) Preparation and characterization of nano SiO2@CeO2 extracted from blast furnace slag and uranium extraction waste for wastewater treatment. Ceram Int 45:7309–7317. https://doi.org/10.1016/j.ceramint.2019.01.014

Fukumura T, Akane S, Sambandan E (2017) Radical detection and mechanism of WO3/CeO2 nanocomposite as a visible active photocatalyst. React Kinet Mech Catal 121:785–795. https://doi.org/10.1007/s11144-017-1182-2

Girase B, Depan D, Shah JS et al (2011) Silver–clay nanohybrid structure for effective and diffusion-controlled antimicrobial activity. Mater Sci Eng, C 31:1759–1766. https://doi.org/10.1016/j.msec.2011.08.007

Gour A, Jain NK (2019) Advances in green synthesis of nanoparticles. Artif Cells Nanomed Biotechnol 47:844–851. https://doi.org/10.1080/21691401.2019.1577878

Hezam A, Namratha K, Drmosh QA et al (2017) Synthesis of heterostructured Bi2O3–CeO2–ZnO photocatalyst with enhanced sunlight photocatalytic activity. Ceram Int 43:5292–5301. https://doi.org/10.1016/j.ceramint.2017.01.059

Jeyakanthan M, Subramanian U, Tangsali RB (2018) Enhanced photoluminescence of CoWO4 in CoWO4/PbWO4 nanocomposites. J Mater Sci Mater Electron 29:1914–1924. https://doi.org/10.1007/s10854-017-8101-1

Ke D, Liu H, Peng T et al (2008) Preparation and photocatalytic activity of WO3/TiO2 nanocomposite particles. Mater Lett 62:447–450. https://doi.org/10.1016/j.matlet.2007.05.060

Koli VB, Kim J-S (2019) Photocatalytic oxidation for removal of gases toluene by TiO2-CeO2 nanocomposites under UV light irradiation. Mater Sci Semicond Process 94:70–79. https://doi.org/10.1016/j.mssp.2019.01.032

Kumar S, Kumar B et al (2013) Synthesis of magnetically separable and recyclable g-C 3 N 4 –Fe 3 O 4 hybrid nanocomposites with enhanced photocatalytic performance under visible-light irradiation. J Phys Chem C 117:26135–26143. https://doi.org/10.1021/jp409651g

Lan S, Sheng X, Lu Y et al (2018) Modification of antibacterial ZnO nanorods with CeO2 nanoparticles: role of CeO2 in impacting morphology and antibacterial activity. Colloid Interface Sci Commun 26:32–38. https://doi.org/10.1016/j.colcom.2018.08.002

Li J-J, Yu E-Q, Cai S-C et al (2019) Noble metal free, CeO2/LaMnO3 hybrid achieving efficient photo-thermal catalytic decomposition of volatile organic compounds under IR light. Appl Catal B 240:141–152. https://doi.org/10.1016/j.apcatb.2018.08.069

Li X, Lin H, Chen X et al (2016) Dendritic α-Fe 2 O 3 /TiO 2 nanocomposites with improved visible light photocatalytic activity. Phys Chem Chem Phys 18:9176–9185. https://doi.org/10.1039/C5CP06681F

Liang Y, Wang SH, Guo PF (2017) Effects of Ag on the photocatalytic activity of multiple layer TiO2 films. Mater Technol 32:46–51. https://doi.org/10.1080/10667857.2015.1116821

Liu W, Zhou J, Hu Z (2019) Nano-sized g-C3N4 thin layer @ CeO2 sphere core-shell photocatalyst combined with H2O2 to degrade doxycycline in water under visible light irradiation. Sep Purif Technol 227:115665. https://doi.org/10.1016/j.seppur.2019.06.003

Lu X, Li X, Chen F et al (2020) Biotemplating synthesis of N-doped two-dimensional CeO2–TiO2 nanosheets with enhanced visible

light photocatalytic desulfurization performance. J Alloy Compd 815:152326. https://doi.org/10.1016/j.jallcom.2019.152326
Ma R, Zhang S, Wen T et al (2019) A critical review on visible-light-response CeO2-based photocatalysts with enhanced photooxidation of organic pollutants. Catal Today 335:20–30. https://doi.org/10.1016/j.cattod.2018.11.016
Misra RDK, Girase B, Depan D, Shah JS (2012) Hybrid nanoscale architecture for enhancement of antimicrobial activity: immobilization of silver nanoparticles on thiol-functionalized polymer crystallized on carbon nanotubes. Adv Eng Mater 14:B93–B100. https://doi.org/10.1002/adem.201180081
Negi K, Kumar M, Chauhan MS (2019) Solution combustion synthesis of CeO2/ZnO nano-composite as a potential scaffold for detection and degradation of p-nitrophenol. Mater Chem Phys 226:59–65. https://doi.org/10.1016/j.matchemphys.2018.12.083
Pourmasoud S, Eghbali-Arani M, Ahmadi F, Rahimi-Nasrabadi M (2017) Synthesis, characterization, and morphological control of PbWO4 nanostructures through precipitation method and its photocatalyst application. J Mater Sci Mater Electron 28:17089–17097. https://doi.org/10.1007/s10854-017-7635-6
Priyadharsan A, Vasanthakumar V, Karthikeyan S et al (2017) Multifunctional properties of ternary CeO2/SnO2/rGO nanocomposites: visible light driven photocatalyst and heavy metal removal. J Photochem Photobiol A 346:32–45. https://doi.org/10.1016/j.jphotochem.2017.05.030
Qi Y, Ye J, Zhang S et al (2019) Controllable synthesis of transition metal ion-doped CeO2 micro/nanostructures for improving photocatalytic performance. J Alloy Compd 782:780–788. https://doi.org/10.1016/j.jallcom.2018.12.111
Rajendran R, Jayaraman V, Varadharajan K (2019) Fabrication of CdS PbWO4 nanocomposite to improve the photocatalytic degradation efficiency of methylene blue under visible light irradiation. J Phys Chem Solids 129:261–269. https://doi.org/10.1016/j.jpcs.2019.01.015
Ramasamy Raja V, Karthika A, Lok Kirubahar S et al (2019) Sonochemical synthesis of novel ZnFe2O4/CeO2 heterojunction with highly enhanced visible light photocatalytic activity. Solid State Ion 332:55–62. https://doi.org/10.1016/j.ssi.2018.12.016
Ramos-Corella KJ, Sotelo-Lerma M, Gil-Salido AA et al (2019) Controlling crystalline phase of TiO 2 thin films to evaluate its biocompatibility. Mater Technol 34:455–462. https://doi.org/10.1080/10667857.2019.1576821
Rana S, Rawat J, Misra RDK (2005a) Anti-microbial active composite nanoparticles with magnetic core and photocatalytic shell: TiO2-NiFe2O4 biomaterial system. Acta Biomater 1:691–703. https://doi.org/10.1016/j.actbio.2005.07.007
Rana S, Rawat J, Misra RDK (2005b) Anti-microbial active composite nanoparticles with magnetic core and photocatalytic shell: TiO2–NiFe2O4 biomaterial system. Acta Biomater 1:691–703. https://doi.org/10.1016/j.actbio.2005.07.007
Rana S, Rawat J, Sorensson MM, Misra RDK (2006) Antimicrobial function of Nd3+-doped anatase titania-coated nickel ferrite composite nanoparticles: a biomaterial system. Acta Biomater 2:421–432. https://doi.org/10.1016/j.actbio.2006.03.005
Ravishankar TN, Ramakrishnappa T, Nagaraju G, Rajanaika H (2015) Synthesis and characterization of CeO 2 nanoparticles via solution combustion method for photocatalytic and antibacterial activity studies. ChemistryOpen 4:146–154. https://doi.org/10.1002/open.201402046
Rawat J, Rana S, Sorensson MM, Misra RDK (2007a) Anti-microbial activity of doped anatase titania coated nickel ferrite composite nanoparticles. Mater Sci Technol 23:97–102. https://doi.org/10.1179/174328407X158488
Rawat J, Rana S, Srivastava R, Misra RDK (2007b) Antimicrobial activity of composite nanoparticles consisting of titania photocatalytic shell and nickel ferrite magnetic core. Mater Sci Eng C 27:540–545. https://doi.org/10.1016/j.msec.2006.05.021
Reddy Yadav LS, Lingaraju K, Daruka Prasad B et al (2017) Synthesis of CeO2 nanoparticles: photocatalytic and antibacterial activities. Eur Phys J Plus 132:239. https://doi.org/10.1140/epjp/i2017-11462-4
Reddy Yadav LS, Manjunath K, Archana B et al (2016) Fruit juice extract mediated synthesis of CeO2 nanoparticles for antibacterial and photocatalytic activities. Eur Phys J Plus 131:154. https://doi.org/10.1140/epjp/i2016-16154-y
Rohini BS, Nagabhushana H, Darshan GP et al (2017) Fabricated CeO2 nanopowders as a novel sensing platform for advanced forensic, electrochemical and photocatalytic applications. Appl Nanosci 7:815–833. https://doi.org/10.1007/s13204-017-0611-x
Rožić L, Petrović S, Lončarević D et al (2019) Influence of annealing temperature on structural, optical and photocatalytic properties of TiO2-CeO2 nanopowders. Ceram Int 45:2361–2367. https://doi.org/10.1016/j.ceramint.2018.10.153
Saravanakumar K, Muthupoongodi S, Muthuraj V (2019) A novel n-CeO2/n-CdO heterojunction nanocomposite for enhanced photodegradation of organic pollutants under visible light irradiation. J Rare Earths 37:853–860. https://doi.org/10.1016/j.jre.2018.12.009
Saravanakumar K, Ramjan MM, Suresh P, Muthuraj V (2016) Fabrication of highly efficient visible light driven Ag/CeO2 photocatalyst for degradation of organic pollutants. J Alloy Compd 664:149–160. https://doi.org/10.1016/j.jallcom.2015.12.245
Shanmugam V, Jeyaperumal KS, Mariappan P, Muppudathi AL (2020) Fabrication of novel g-C3N4based MoS2and Bi2O3nanorod embedded ternary nanocomposites for superior photocatalytic performance and destruction of bacteria. New J Chem 44:13182–13194. https://doi.org/10.1039/d0nj02101f
Shanmugam V, Sanjeevamuthu S, Jeyaperumal KS, Vairamuthu R (2019) Fabrication of heterostructured vanadium modified g-C 3 N 4 /TiO 2 hybrid photocatalyst for improved photocatalytic performance under visible light exposure and antibacterial activities. J Ind Eng Chem 76:318–332. https://doi.org/10.1016/j.jiec.2019.03.056
Sunkara BK, Misra RDK (2008) Enhanced antibactericidal function of W4+-doped titania-coated nickel ferrite composite nanoparticles: a biomaterial system. Acta Biomater 4:273–283. https://doi.org/10.1016/j.actbio.2007.07.002
Syed Khadar YA, Balamurugan A, Devarajan VP et al (2019) Synthesis, characterization and antibacterial activity of cobalt doped cerium oxide (CeO2:Co) nanoparticles by using hydrothermal method. J Market Res 8:267–274. https://doi.org/10.1016/j.jmrt.2017.12.005
Tomova D, Iliev V, Eliyas A, Rakovsky S (2015) Promoting the oxidative removal rate of oxalic acid on gold-doped CeO 2 /TiO 2 photocatalysts under UV and visible light irradiation. Sep Purif Technol 156:715–723. https://doi.org/10.1016/j.seppur.2015.10.070
Velusamy P, Lakshmi G (2017) Enhanced photocatalytic performance of (ZnO/CeO2)-β-CD system for the effective decolorization of Rhodamine B under UV light irradiation. Appl Water Sci 7:4025–4036. https://doi.org/10.1007/s13201-017-0554-0
Venkatasubramanian R, Srivastava RS, Misra RDK (2008) Comparative study of antimicrobial and photocatalytic activity in titania encapsulated composite nanoparticles with different dopants. Mater Sci Technol 24:589–595. https://doi.org/10.1179/174328408X282065
Vignesh S, Suganthi S, Kalyana Sundar J, Raj V (2019) Construction of α-Fe2O3/CeO2 decorated g-C3N4 nanosheets for magnetically separable efficient photocatalytic performance under visible light exposure and bacterial disinfection. Appl Surf Sci 488:763–777. https://doi.org/10.1016/j.apsusc.2019.05.147

Wang K, Su P, Li H et al (2019) Synthesis, characterization and antimicrobial activity of hybrid-structured Ag@CeO2 nanoparticles. Chem Pap 73:1279–1286. https://doi.org/10.1007/s11696-019-00681-5

Wang Y, Tian H (2020) Study on the construction of YMnO3/CeO2 composite photocatalyst heterostructure and photocatalytic degradation of methyl red. Optik 201:163524. https://doi.org/10.1016/j.ijleo.2019.163524

Wei H, Wang L, Li Z et al (2014) Synthesis and photocatalytic activity of one-dimensional CdS@TiO2 core-shell heterostructures. Nano-Micro Lett 3:6–11. https://doi.org/10.1007/bf03353645

Wen X-J, Niu C-G, Zhang L et al (2018) A novel Ag2O/CeO2 heterojunction photocatalysts for photocatalytic degradation of enrofloxacin: possible degradation pathways, mineralization activity and an in depth mechanism insight. Appl Catal B 221:701–714. https://doi.org/10.1016/j.apcatb.2017.09.060

Xian T, Yang H, Di LJ, Dai JF (2015) Enhanced photocatalytic activity of BaTiO3@g-C3N4 for the degradation of methyl orange under simulated sunlight irradiation. J Alloy Compd 622:1098–1104. https://doi.org/10.1016/j.jallcom.2014.11.051

Xiong Y, Wang B, Hu W, Dai L (2015) Facile synthesis and characterization of erythrocyte-like Y-doped PbWO4 mesocrystals and their photocatalytic activity. Mater Charact 105:24–29. https://doi.org/10.1016/j.matchar.2015.04.016

Xu J, Li M, Qiu J et al (2020) PEGylated deep eutectic solvent-assisted synthesis of CdS@CeO2 composites with enhanced visible light photocatalytic ability. Chem Eng J 383:123135. https://doi.org/10.1016/j.cej.2019.123135

Xu L, Wang J (2012) Magnetic nanoscaled Fe 3 O 4 /CeO 2 composite as an efficient fenton-like heterogeneous catalyst for degradation of 4-chlorophenol. Environ Sci Technol 46:10145–10153. https://doi.org/10.1021/es300303f

Yu C, Bai Y, He H et al (2015) Synthesis, characterization and photocatalytic performance of rod-shaped Pt/PbWO4 composite microcrystals. Chin J Catal 36:2178–2185. https://doi.org/10.1016/S1872-2067(15)61009-9

Yu C, Cao F, Li X et al (2013) Hydrothermal synthesis and characterization of novel PbWO4 microspheres with hierarchical nanostructures and enhanced photocatalytic performance in dye degradation. Chem Eng J 219:86–95. https://doi.org/10.1016/j.cej.2012.12.064

Yue D, Chen D, Lu W et al (2016) Enhanced photocatalytic performance and morphology evolvement of PbWO 4 dendritic nanostructures through Eu 3+ doping. RSC Adv 6:81447–81453. https://doi.org/10.1039/C6RA15045D

Zeleke MA, Kuo D-H (2019) Synthesis and application of V2O5-CeO2 nanocomposite catalyst for enhanced degradation of methylene blue under visible light illumination. Chemosphere 235:935–944. https://doi.org/10.1016/j.chemosphere.2019.06.230

Zhang J, Peng L-L, Tang Y, Wu H (2017) Convenient synthesis of twin-Christmas tree-like PbWO4 microcrystals and their photocatalytic properties. Front Mater Sci 11:139–146. https://doi.org/10.1007/s11706-017-0381-0

Zhang M, Zhang C, Zhai X et al (2019a) Antibacterial mechanism and activity of cerium oxide nanoparticles. Sci China Mater 62:1727–1739. https://doi.org/10.1007/s40843-019-9471-7

Zhang Q-P, Liang D-M, Zhu W-F et al (2019b) Fabrication of h-BN@PbWO4 with a facile sol-gel method towards enhanced photocatalytic and radiation shielding properties. J Solid State Chem 269:594–599. https://doi.org/10.1016/j.jssc.2018.10.043